Bidirectional Bacterial Gliding Motility Powered by the Collective Transport of Cell Surface Proteins

Hirofumi Wada,[1] Daisuke Nakane,[2] and Hsuan-Yi Chen[3]

[1]*Department of Physics, Ritsumeikan University, Kusatsu, 525-8577 Shiga, Japan*
[2]*Department of Physics, Gakushuin University, Toshima, 171-8588 Tokyo, Japan*
[3]*Department of Physics, National Central University, Jhongli, 32001 Taiwan, Republic of China;*
Physics Division, National Center for Theoretical Sciences, Hsinchu, 30113 Taiwan, Republic of China
and Institute of Physics, Academia Sinica, Taipei, 11529 Taiwan, Republic of China
(Received 21 June 2013; published 11 December 2013)

The gliding motility of *Flavobacterium johnsoniae* is driven by moving surface adhesive proteins. Recently, these motility components were observed to travel along a closed loop on the cell surface. The mechanism by which such moving surface adhesins give rise to cell motion remains unknown. On the basis of the unique motility properties of *F. johnsoniae*, we present a generic model for bidirectional motion of rigidly coupled adhesins, which are propelled in opposite directions. Using analytical and numerical methods, we demonstrate that, for a sufficiently large adhesin speed, bidirectional motion arises from spontaneous symmetry breaking. The model also predicts that, close to the bifurcation point, a weak asymmetry in the binding dynamics is sufficient to facilitate directed motility, indicating that the direction of motion could be sensitively regulated internally in response to inhomogeneity of the environment.

Cell motility is the result of coordination among a large number of constituent processive motors and biomolecules [1]. A general understanding of such a coordination mechanism is currently a central topic in biological physics [2–5].

The movement of a bacterium over a solid surface such as glass or hard agar without flagella is referred to as gliding motility [6,7]. Cells of *Flavobacterium johnsoniae* move rapidly over surfaces at speeds of 1–3 μm/s, but the exact mechanism underlying such rapid motion is poorly understood [8,9]. Recently, fluorescence microscopy analysis of single *F. johnsoniae* cells revealed that the thin, 150-nm filaments of the surface protein SprB, which extend from the cell surface [10], are propelled at approximately 2 μm/s along a closed helical loop track with a pitch angle ~20° (Fig. 1) [11]. The cells also show bidirectional motility, reversing the direction stochastically with similar speeds in both directions. Cell motility is achieved in such a way that the SprBs traveling toward the rear of the cell attach to the substrate, while those traveling toward the front of the cell are detached. However, the precise orchestration of this coordination of many moving adhesins is currently unknown.

On the basis of these observations, in this Letter, we present a generic model for bidirectional motion of rigidly coupled adhesins propelled in opposing directions. Using a stochastic simulation and a rate equation approach, we demonstrate that bidirectional motion is a collective behavior of many traveling adhesins. By increasing the speed of the adhesins, a transition from a rest state to a moving state occurs through a pitchfork bifurcation, causing spontaneous symmetry breaking.

To focus on the linear motion of the bacterium, we construct a one-dimensional model for the bidirectional motion of a cell along its long axis. The possible rotation of the bacterium due to the helical nature of the adhesin track is therefore ignored. In our model, the SprB molecules in contact with the substrate move along the plus $(+)$ and minus $(-)$ subtracks as shown in Fig. 2. Once a SprB binds to the substrate, traction force acts on the substrate because of the motion of the adhesin. Based on experimental observations, we assume that the SprB molecules move at a constant speed v_0 [12] and the switching of the moving directions occurs only at the two poles of a cell. Therefore, the adhesin traffic is uniform and unidirectional on each subtrack. This ensures the same number of adhesins N in
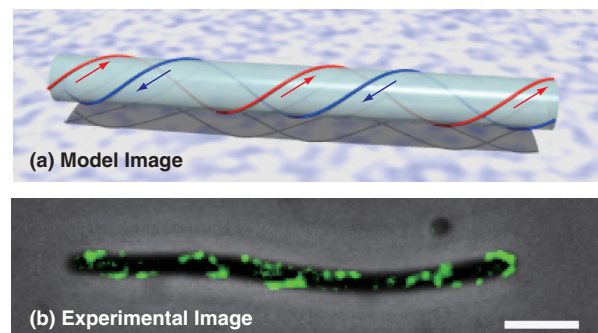
FIG. 1 (color online).   (Top) Model image: Left-handed closed helical loop model for the gliding motility of a bacterium. (Bottom) Helical localization of the surface protein SprB. The immunofluorescence image of SprB (green) was merged with the phase-contrast image of a *F. johnsoniae* cell. Scale bar: 2 μm.
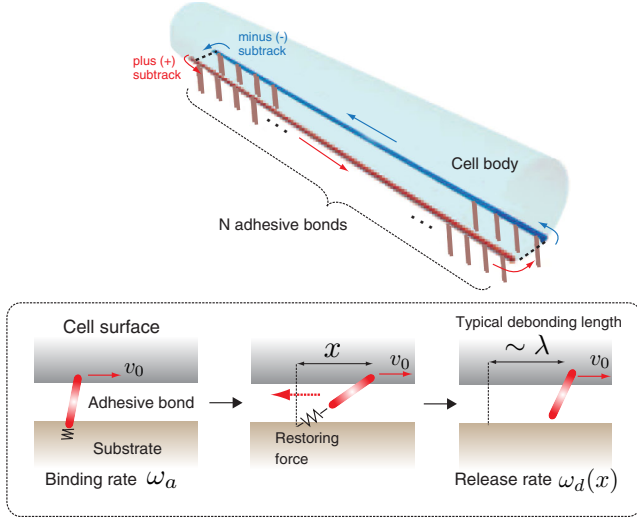
FIG. 2 (color online). Geometry of our one-dimensional model. Only the translational motion of motor-driven adhesive proteins along a cell's long axis is considered. There are the same number N of adhesins on the plus ($+$) and minus ($-$) subtracks. (Bottom) A typical sequence of binding and release dynamics of moving adhesins.

the plus and minus subtracks under the assumption of a train of equidistant SprB proteins on the track.

In reality, SprBs move along a helical track around a bacterium. Thus, the number of SprBs close to a substrate is smaller than the total number of SprBs on the cell surface. The minimal distance between the outer membrane and the substrate was previously estimated to be approximately 100 nm [13]. By considering the length of SprB (~ 150 nm) [11] and using 10 nm as the average distance between neighboring SprBs [14], the maximal number of effective force generators per subtrack in our model is estimated as $N \sim 100$–200 for a cell of typical length of 5–10 μm (for details, see Supplemental Material [15]). In the numerical simulations below, we mainly use $N = 50$.

We employ a simplified two-state model for the force generation by individual adhesins [16]. Upon bond formation, the extension x of a substrate-bound protein increases and a tension $f_\sigma(x)$ develops (Fig. 2). We assume $f_\sigma(x) = \kappa x$ for $\sigma = 1$ (bound) and $f_\sigma(x) = 0$ for $\sigma = 0$ (released), where κ represents an effective elastic modulus. The instantaneous total force exerted by all the bonds on the $\pm$ subtrack is the sum of those restoring forces. A cell body moving at velocity v_c also experiences a friction force $-\Gamma v_c$. Because the inertia is negligible at this small scale, the total force acting on the cell body vanishes:

$$0 = -\sum_{i=1}^{N}(f_{\sigma_i}^{+} + f_{\sigma_i}^{-}) - \Gamma v_c + F_{\text{ext}}, \qquad (1)$$

where an external force F_{ext} is included. To complete our model, we need to specify the transition dynamics between

the states $\sigma = 0$ and $\sigma = 1$. A free bond ($\sigma = 0$) undergoes binding transition to the bound state ($\sigma = 1$) with a constant probability rate ω_a. While binding occurs only at $x = 0$, the probability rate ω_d for the dissociation of the bond depends on x. Assuming the bound state forms a deep potential well and the energy barrier for bond dissociation decreases linearly with the force $f_\sigma(x)$, we use Bell's expression [17] $\omega_d(x) = \omega_0 \exp[f_\sigma(|x|)/(\kappa\lambda)]$, where λ characterizes the length at which a bond is typically detached from a substrate.

We first present an analytical argument based on a rate equation. Let the number of closed bonds on the $\pm$ subtrack at t with extension x be $n_\pm(x, t)$. The conservation of the number of bonds suggests the dynamic equation for $n_\pm(x, t)$:

$$\dot{n}_\pm + v_\pm \partial_x n_\pm = -\omega_d(x)n_\pm + \omega_a \delta(x)\left[N - \int_\pm n_\pm dx\right], \qquad (2)$$

where the dot denotes the time derivative and $\delta(x)$ is the delta function. $v_\pm = \pm v_0 + v_c$ are the velocities of the adhesins relative to the substrate, and $\int_\pm$ in Eq. (2) represents the integration over the range that x can take. Since fluctuations are neglected, v_c varies between $-v_0$ and v_0, and therefore $v_+ > 0$ and $v_- < 0$. Because $\dot{x} = v_\pm$ for the $\pm$ subtrack, respectively, $0 \leq x < \infty$ for the plus bonds, while $-\infty < x \leq 0$ for the minus bonds. At the steady state, Eq. (2) is readily solved [18] to yield $n_\pm(x) = A_\pm \exp[-v_\pm^{-1} \int_0^x \omega_d(x')dx']$, where $A_\pm = \pm(\omega_a N/v_\pm)\{1 + \omega_a/v_\pm \int_\pm dx \exp[-v_\pm^{-1}\int_0^x \omega_d(x')dx']\}^{-1}$. By introducing the rescaled variables $z = |x|/\lambda$ and $\hat{v} = v_c/v_0$, the rescaled form of Eq. (1) becomes

$$\hat{f}_{\text{ext}} = \frac{\mu_1^+(\hat{v})}{\beta(1 + \hat{v}) + \mu_0^+(\hat{v})} - \frac{\mu_1^-(\hat{v})}{\beta(1 - \hat{v}) + \mu_0^-(\hat{v})} + \Xi\beta\hat{v}, \qquad (3)$$

where $\Xi = \Gamma\omega_a/(N\kappa)$ is the rescaled hydrodynamic drag coefficient and $\hat{f}_{\text{ext}} = F_{\text{ext}}/(N\kappa\lambda)$. In Eq. (3), we have introduced the characteristic function $\mu_n^\pm(v) = \int_0^\infty z^n \exp[-\frac{r}{\beta}(e^z - 1)/(1 \pm v)]dz$, for $n = 0, 1, 2, \ldots$. Note that the total force exerted by all the bonds on one subtrack is calculated according to $F_\pm = \int_\pm \kappa x n_\pm(x)dx$, leading to $F_\pm = \pm\kappa\lambda N\mu_1^\pm(\hat{v})/[\beta(1 \pm \hat{v}) + \mu_0^\pm(\hat{v})]$. A nondimensional parameter, $\beta = v_0/(\omega_a\lambda)$, controls the cell dynamics. The binding and unbinding equilibrium of the bonds leads to $r = \omega_0/\omega_a = \exp(-E_a/k_BT)$. Assuming that the binding energy between an SprB and the substrate E_a is typically 2–3k_BT (k_BT is thermal energy), we will mainly use $r = 0.1$.

Equation (3) is plotted in Fig. 3(a) for $r = 0.1$. The force-velocity curve is monotonic for small β [15,19]. For large β, the curve becomes S shaped, and we can calculate two nontrivial solutions for $\hat{f}_{\text{ext}} = 0$. This indicates that a cell starts to move via spontaneous symmetry breaking beyond a
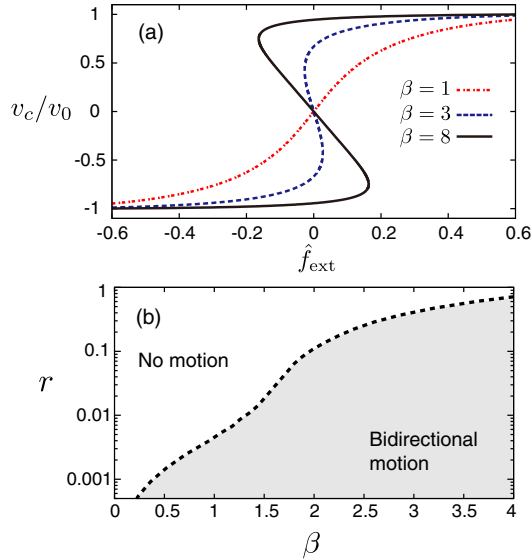
FIG. 3 (color online).   Predictions obtained from Eq. (3):
(a) Force-velocity curves for $r = 0.1$ and different values of β.
(b) State diagram on the βr plane. $\Xi = 2 \times 10^{-3}$ in (a) and (b).

certain critical value of β. Experimentally, the two parameters β and r vary together. Thus, we show in Fig. 3(b) the state diagram on the βr plane.

To determine the effects of a finite number of bonds and switching dynamics of the bidirectional motion, we performed numerical simulations of a rigidly coupled $2N$-moving bonds system. For details, see Ref. [15]. In Fig. 4(a), the instantaneous cell velocity $\hat{v}$ for $N = 50$ is plotted as a function of time in the absence of external loading. While the cell's velocity v_c fluctuates around zero

for $\beta = 0.5$, v_c switches stochastically between values of magnitude $\sim v_0$ of opposite sign at larger β, clearly suggesting a bidirectional motion.

Figure 4(b) shows the cell velocity as a function of β for $\hat{f}_{ext} = 0$. A numerically obtained velocity histogram is fitted to Gaussian distributions (some of which are shown in the insets), from which its mean value and standard deviations are extracted. The agreement between the simulation data and the prediction from the theory [solid line in Fig. 4(b)] is good [20].

The total forces exerted by all the bonds on $\pm$ subtracks, $F_\pm$, are plotted as a function of β in Fig. 4(c). Here we redefined the "+" direction to be the direction of cell movement; thus, $v_c \geq 0$ for all cells, and the magnitude of F_- is always not less than the magnitude of F_+. At the bifurcation, $F_\pm$ starts to differ, and the difference increases with β, consistent with the results from real bacteria. Figure 4(c) shows that such asymmetry can emerge spontaneously through a dynamic instability due to force-dependent detachment rates and coupling between the bonds. The inset shows an exponential growth of the switching time T_{sw} [15] with β, a reasonable result for broken symmetry in finite N systems.

Figure 4(d) shows that T_{sw} increases exponentially with N. Since the number of SprBs should be proportional to the cell length, this result can be tested in experiments for cells with different lengths [21]. On the other hand, the inset in Fig. 4(d) shows that the cell velocity is insensitive to N, in agreement with the experimental observation [8]. The dependence of the cell velocity on the hydrodynamic drag coefficient Ξ is shown in Fig. 4(e). Our calculation predicts that cell motion disappears above a certain value
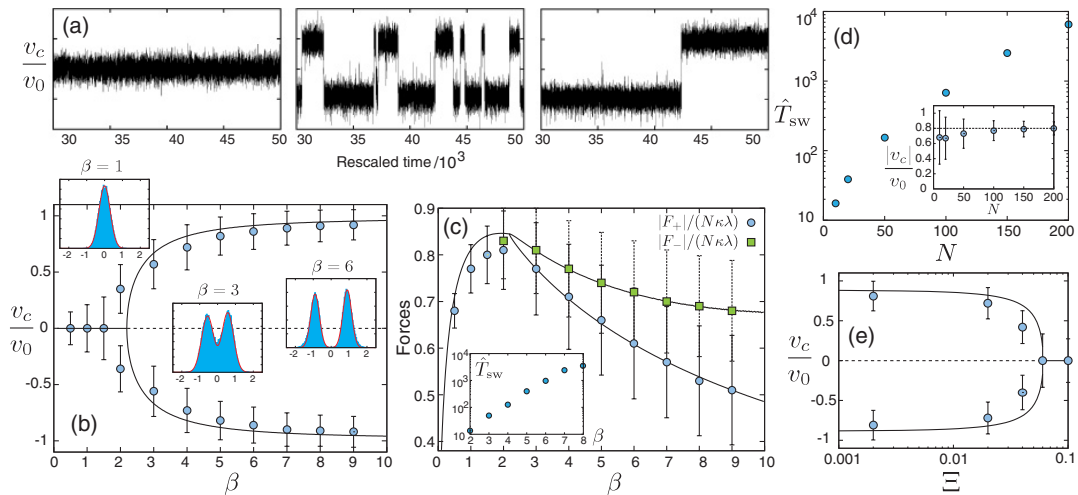
FIG. 4 (color online).   (a) Rescaled cell velocity as a function of time obtained in our simulations. From left to right, $\beta = 0.5, 6$, and 9. (b) Motility diagram: Comparison of our analytical predictions (solid and dashed lines) and the numerical data obtained from the simulations (filled blue circles). (c) Total force exerted by the two subtracks on the substrate, $F_\pm$ (rescaled by $N\kappa\lambda$), plotted against β. Here, $v_c \geq 0$; thus, $|F_+| \leq |F_-|$. Inset: The rescaled characteristic switching time $\hat{T}_{sw}$ plotted as a function of β. (d) $\hat{T}_{sw}$ plotted as a function of N for $\beta = 4$. Inset: v_c/v_0 as a function of N, for $\beta = 4$. (e) v_c/v_0 plotted against the rescaled drag coefficient Ξ, for $\beta = 4$ and $N = 50$. In both (b) and (c), the error bars indicate the standard deviations of the velocity and force histograms. In (b)–(e), solid and dashed lines represent the analytical predictions. For all the data shown, $r = 0.1$ and $\Xi = 2 \times 10^{-3}$ [except (e)].
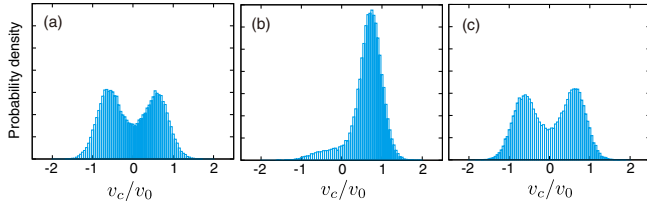
FIG. 5 (color online). Dstribution of the cell velocity close to the bifurcation $\beta_- = 3$ (and $N = 50$). (a) Symmetric case $(\beta_+/\beta_- = 1)$ and $\hat{f}_{ext} = 0$, (b) asymmetric case $(\beta_+/\beta_- = 1.15)$ and $\hat{f}_{ext} = 0$, and (c) asymmetric case $\beta_+/\beta_- = 1.15$ and $\hat{f}_{ext} = -0.05$.

of Ξ, which can be tested in experiments by increasing the medium viscosity.

In the symmetric situation studied above, the net velocity of a cell over a long time is zero. Clearly, a cell with chemotactic behavior needs to facilitate its motion in the direction of the chemoattractant. Here, we consider the possibility in which the asymmetry is introduced through the difference in the binding rates between the subtracks. Other mechanisms may also lead to a similar asymmetry. Because intracellular processes for the chemotaxis of *F. johnsoniae* is currently unknown, we confine this analysis to a hypothesized reaction asymmetry, which can be characterized by ω_a^-/ω_a^+ or β_+/β_-. In Figs. 5(b) and 5(c), the velocity histograms obtained for $\beta_+/\beta_- = 1.15$ (with $\beta_- = 3$) in the absence and presence of external forces are shown. Without external force, the distribution is monotonic and sharply peaks at $v_c \sim v_0$ [Fig. 5(b), compared to the symmetric case shown in Fig. 5(a)]. The bistable nature is observed only when an external force is exerted on the cell [Fig. 5(c)]. This result suggests that a sufficiently small asymmetry should facilitate the motion of a cell toward a specific direction. Here, the cooperativity of many propelling adhesins is at play to enhance and amplify the weak asymmetry. It is worth noticing that similar amplification mechanisms are likely to be common in biological sensory systems such as the cochlea of the inner ear [22–25]. Here, we propose that, by tuning $v_0/(\omega_a\lambda)$ close to a pitchfork bifurcation, the motion of a cell can be guided by a small gradient of chemoattractant concentration. This prediction may be further pursued experimentally by modulating the affinity of SprB for a substrate by changing the physicochemical properties of the substrate.

For *F. johnsoniae*, the SprB speed $v_0 \sim 2$ μm/s and the cell speed $v_c \sim 2$ μm/s have been experimentally established [11]. A cell body is a cylinder of length $L \sim 5$–10 μm and of width $a \sim 200$ nm, while SprB is a filament of length ~150 nm and of width ~5 nm [11,14]. Since a fluid layer is present between the cell surface and the substrate, for a rough estimate of Γ, we use the Stokes friction of a cylindrical cell body $\Gamma \approx 2\pi\eta L/\ln(L/a)$. Assuming a water viscosity $\eta \sim 10^{-3}$ kg/s m, and $\kappa \sim 10^2$ pN/μm [26], we obtain

$\Xi \sim 10^{-3}$–10^{-4}, consistent with the values we used. From Fig. 4(c), the typical switching time interval T_{sw} can be read as $T_{sw} \sim 200$–$2000 \times \lambda/v_0$. Assuming $\lambda \sim 5$–10 nm, we have $T_{sw} \sim 1$–10 s, consistent with the switching time of a few seconds observed in the experiment [11]. To have $\beta = 4$ and $r = 0.1$, we suggest $\omega_a = 100$ s^{-1} and $\omega_0 = 10$ s^{-1}, comparable to the values used in other studies [27]. Therefore, our parameters are relevant to those of the real biological situations.

Our model shares some features with collective motor models for muscles [28], directed motion in motility assays [27], spindle oscillations [29], and the tug-of-war model for cargo transport by molecular motors [30]. While individual motors were included explicitly in the above-mentioned models, in our model the driving force is specified by a single parameter v_0. Furthermore, in the tug-of-war model, two groups of motors exert forces in opposite directions and the motors in the same group share equal force; this is different from our model, in which the force of each adhesin is determined by its elongation, which depends on when it binds to the substrate. On the other hand, in the bidirectional motility proposed in Ref. [27], each motor can exert a force in either direction, which is clearly different from our case in which the direction of the force from an adhesin is completely determined by its subtrack.

F. johnsoniae cells also show other types of motions such as flipping and pivoting, for which transient clustering of SprB at cell poles may be responsible [21]. In addition, a cell body rotation resulting from the helical nature of the SprB trafficking may affect the coordination between the oppositely moving proteins and directional control of cells. Clearly, an important next step is to incorporate these three-dimensional features into the present simplified description.

Recently, *Mxyococcus xanthus* was found to show a similar motility (termed "adventurous motility"), in which motility motors are proposed to travel along a closed helical loop in the cytoplasm or cytoplasmic membrane [31–34]. Although *M. xanthus* is biologically distinct from *F. johnsoniae*—it belongs to a different phylum of bacteria and moves 50–100 times slower than *F. johnsoniae* cells— their common motility features may reflect the general physical mechanism leading to the convergent evolution of analogous systems. Further studies are necessary to explore these exciting aspects.

[1] D. Bray, *Cell Movement: From Molecules to Motility* (Garland, New York, 2001).
[2] S. Leibler and D. Huse, J. Cell Biol. **121**, 1357 (1993).
[3] F. Julicher and J. Prost, Phys. Rev. Lett. **75**, 2618 (1995).

[4] E. Tjhung, D. Marenduzzo, and M. E. Cates, Proc. Natl. Acad. Sci. U.S.A. **109**, 12381 (2012).

[5] C. W. Wolgemuth, O. Igoshin, and G. Oster, Biophys. J. **85**, 828 (2003).

[6] J. Henrichsen, Bacteriol. Rev. **36**, 478 (1972).

[7] M. Miyata, Annu. Rev. Microbiol. **64**, 519 (2010).

[8] I. R. Lapidus and H. C. Berg, J. Bacteriol. **151**, 384 (1982).

[9] K. F. Jarrell and M. J. McBride, Nat. Rev. Microbiol. **6**, 466 (2008).

[10] S. S. Nelson, S. Bollampalli, and M. J. McBride, J. Bacteriol. **190**, 2851 (2008).

[11] D. Nakane, K. Sato, H. Wada, M. J. McBride, and K. Nakayama, Proc. Natl. Acad. Sci. U.S.A. **110**, 11145 (2013).

[12] In the experiment by Lapidus and Berg [8], it was observed that polystyrene beads bound to the cell surface were propelled at about 2 μm/s. Small spheres were found to move at about the same speed as large spheres, even though the viscous drag exerted by the external medium varies by a factor of 10 or more, indicating that the rate of movement is not limited by the external load.

[13] S. L. Godwin, M. Fletcher, and R. P. Burchard, J. Bacteriol. **171**, 4589 (1989).

[14] J. Liu, M. J. McBride, and S. Subramaniam, J. Bacteriol. **189**, 7503 (2007).

[15] See Supplemental Material at for http://link.aps.org/supplemental/10.1103/PhysRevLett.111.248102 for details of our model and the simulation method.

[16] A. F. Huxley, Prog. Biophys. Biophys. Chem. **7**, 255 (1957).

[17] G. I. Bell, Science **200**, 618 (1978).

[18] K. Sato and A. Toda, J. Phys. Soc. Jpn. **68**, 77 (1999).

[19] K. Tawada and K. Sekimoto, J. Theor. Biol. **150**, 193 (1991).

[20] The simulation results close to the transition point are somewhat different from our theory owing to the fluctuations arising from the relatively small number of bonds. We confirmed that the analytic prediction becomes exact in the limit of large N (data not shown), for which the fluctuations and the reversal of the direction of motion are negligible.

[21] P. J. Beatson and K. C. Marshall, Canadian Journal of Microbiology **40**, 173 (1994).

[22] T. Gold, Proc. R. Soc. Lond. B **135**, 492 (1948).

[23] T. A. J. Duke and D. Bray, Proc. Natl. Acad. Sci. U.S.A. **96**, 10104 (1999).

[24] S. Camalet, T. Duke, F. Julicher, and J. Prost, Proc. Natl. Acad. Sci. U.S.A. **97**, 3183 (2000).

[25] V. M. Eguiluz, M. Ospeck, Y. Choe, A. J. Hudspeth, and M. O. Magnasco, Phys. Rev. Lett. **84**, 5232 (2000).

[26] J. Chen, J. Neu, M. Miyata, and G. Oster, Biophys. J. **97**, 2930 (2009).

[27] M. Badoual, F. Julicher, and J. Prost, Proc. Natl. Acad. Sci. U.S.A. **99**, 6696 (2002).

[28] T. Duke, Phil. Trans. R. Soc. B **355**, 529 (2000).

[29] S. W. Grill, K. Kruse, and F. Julicher, Phys. Rev. Lett. **94**, 108104 (2005).

[30] M. J. L. Muller, S. Klumpp, and R. Lipowsky, Proc. Natl. Acad. Sci. U.S.A. **105**, 4609 (2008).

[31] T. Mignot, J. W. Shaevitz, P. L. Hartzell, and D. R. Zusman, Science **315**, 853 (2007).

[32] M. Sun, M. Wartel, E. Cascales, J. W. Shaevitz, and T. Mignot, Proc. Natl. Acad. Sci. U.S.A. **108**, 7559 (2011).

[33] B. Nan, J. Chen, J. C. Neu, R. M. Berry, G. Oster, and D. R. Zusman, Proc. Natl. Acad. Sci. U.S.A. **108**, 2498 (2011).

[34] Another model for *M. xanthus* gliding motility proposes that the hydration of slime gel from the rear of the cell is the force-generating mechanism: C. Wolgemuth, E. Hoiczyk, D. Kaiser, and G. Oster, Curr. Biol. **12**, 369 (2002).